Cytomimetic Biomaterials. 4. In-Situ Photopolymerization of Phospholipids on an Alkylated Surface

Janine M. Orban,[†] Keith M. Faucher,[§] Richard A. Dluhy,[§] and Elliot L. Chaikof*[,†,‡]

Departments of Surgery and Bioengineering, Emory University School of Medicine, Atlanta, Georgia 30322, School of Chemical Engineering, Georgia Institute of Technology, Atlanta, Georgia 30320, and Department of Chemsitry, University of Georgia, Athens, Georgia

Received September 15, 1999; Revised Manuscript Received February 28, 2000

ABSTRACT: A stable, substrate-supported phospholipid film was created by in-situ photopolymerization of an acrylate functionalized lipid assembly. The lipid film was generated on alkylated substrates by vesicle fusion and polymerized by irradiation with visible light, using eosin Y/triethanolamine as the photoinitiating species. Optimal experimental conditions were determined with respect to vesicle fusion time and duration of irradiation. The resulting polymeric lipid film was characterized by contact angle measurements, angle-resolved ESCA, and polarized external reflectance infrared spectroscopy. Static stability and desorption studies indicate enhanced stability of the photopolymerized system when compared with a heat-initiated analogue prepared by classical free-radical techniques.

Introduction

As part of our program in biomimetic materials and tissue engineering, we have targeted several elements of the arterial wall as structural models for the design of an artificial blood vessel based upon the assembly of component structures. In large measure, the endothelial cell which lines the blood-contacting surface of an artery or vein is responsible for maintaining a thrombus-free environment. While the capability of the endothelial cell to resist biological fouling processes can be attributed, in part, to the release of soluble factors, cell membrane-associated features undoubtedly play a significant and, perhaps, dominant role in this regard. In fact, several investigators have observed that the phosphorylcholine (PC) headgroup limits platelet and plasma protein binding to synthetic surfaces.[1] Typically, the PC functional group has been incorporated into synthetic polymers either by direct surface grafting[2] or as a component part of a monomer species utilized in copolymer synthesis. The latter approach has yielded copolymers with the PC headgroup as a pendant species or, less frequently, within the polymer backbone.[3] As an alternative strategy for designing biologically functional cell membrane-like or cytomimetic systems, we have pursued an approach based upon the stabilization of self-assembled, substrate-supported lipid molecules through a process of in-situ polymerization on planar alkylated surfaces.[4] Significantly, the *modular* nature of this platform, in contrast to other surface modification strategies, provides an enhanced degree of flexibility with respect to incorporation of transmembrane proteins, as well as peptide or carbohydrate lipophilic conjugates. This is considered a critical design constraint since the phosphorylcholine headgroup alone will probably provide only a small improvement in the clinical performance characteristics of blood contacting materials.

While we have previously demonstrated that *nonpolymerized*, multicomponent lipid and lipopeptide assemblies on a solid substrate may exhibit long-term stability in an aqueous environment for periods exceeding 1 month; these systems are unstable as the operating environment becomes more complex.[5] For example, significant lipopeptide loss was noted as the temperature approached the main phase transition temperature (T_m) of the lipid and when proteins or other soluble biomolecules were added to the bathing media. In response to design requirements for both flexible assembly of structurally diverse film constituents and long-term stability of surface properties, we initially polymerized lipid monolayers supported on various alkylated substrates by a heat-initiated free-radical process. Admittedly, a recognized limitation of a thermally initiated polymerization scheme is the inability to incorporate heat-sensitive biomolecules into this assembly. Toward this end, we have found photopolymerization to be a useful technique, as the free-radical process is initiated independent of polymerization temperature. For example, visible-light-mediated photopolymerization has been successfully achieved using the xanthine dye, eosin Y (EY), which was initially characterized by Neckers[6] and colleagues. Significantly, Hubbell[7] and associates have used the eosin Y/triethanolamine (TEA) system for the formation of photopolymerized PEG-acrylate gels. When used for cell encapsulation, a minimal effect on cell viability over a range of laser fluxes (45−180 mW/cm^2) and pulse durations (8−30 s) was observed. The mechanism of initiation involves reductive electron transfer from a donor, commonly TEA, to the dye. A proton is subsequently lost from the TEA radical cation at the α-position to the amine to yield a radical species that serves as the initiator. In extending this strategy to the polymerization of a supported lipid film, we postulated that the TEA radical is small enough to diffuse into a lipid assembly and, thereby, initiate a polymerization reaction. We report, herein, the self-assembly of acrylate functionalized phospholipids on alkylated supports, followed by in-situ polymerization initiated by the irradiation of EY/TEA using an inexpensive quartz halogen lamp (Figure 1).

[†] Emory University School of Medicine.
[‡] Georgia Institute of Technology.
[§] University of Georgia.
* Corresponding author. Phone (404) 727-8413; Fax (404) 727-3660; E-mail echaiko@emory.edu.

10.1021/ma9915780 CCC: $19.00
Published on Web 05/06/2000

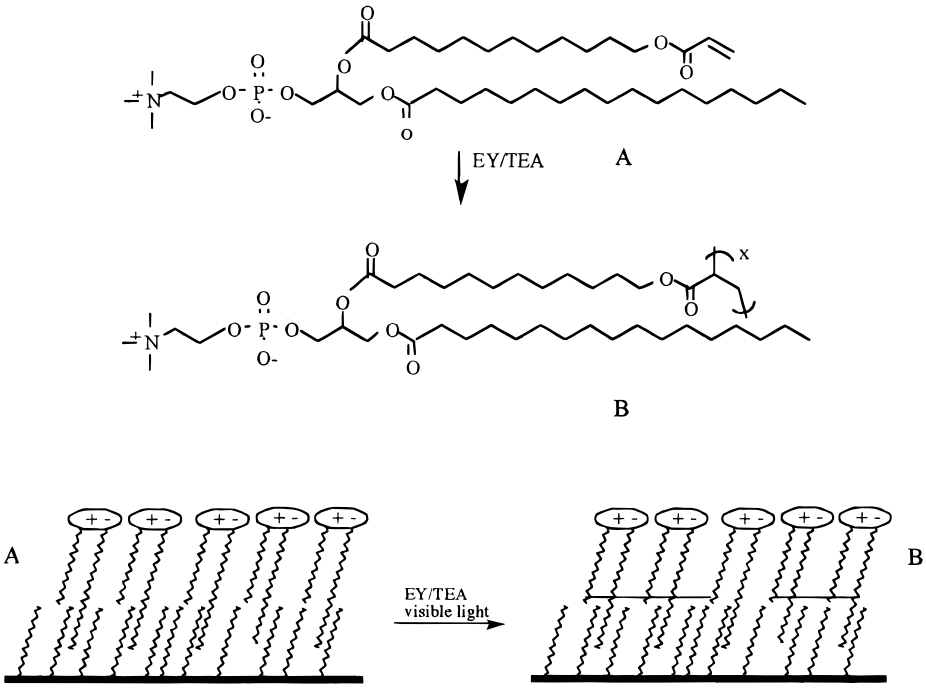

Figure 1. Photopolymerization scheme for the generation of a stabilized, supported, polymeric phospholipid monolayer on an alkylated support.

The resultant substrate-supported poly(phosphatidylcholine) (poly(PC)) film was characterized by contact angle, ESCA, and polarized external infrared spectroscopy. Of note, the photopolymerized system demonstrated enhanced stability when compared with a poly(PC) film polymerized by a heat-initiated free-radical technique.

Experimental Section

Materials. EY (5% in water), TEA, VP (1-vinyl-2-pyrrolidinone) (Aldrich), *n*-octyl-*β*-glucopyranoside (OG; Sigma), and reagent grade water (Baxter) were used as received. Nucleopore polycarbonate filters were obtained from Costar. Acrylate-PC (1-palmitoyl-2-[12-(acryloyloxy)dodeca-noyl]-*sn*-glycero-3-phosphocholine) and OTS (octadecyltrichlorosilanized)-coated glass and silicon (Si) substrates were prepared as previously described.[4]

Instrumentation. Irradiation was performed using a DynaLume quartz halogen illuminator equipped with a heat shield (Scientific Instruments). Light intensity was measured using a radiometer model IL 1400A equipped with a SL021 photodetector and FQI filter (International Light). Contact angle measurements were performed using a Ramé-Hart NRL C.A. goniometer model 100-00-115 with 0.45 μm filtered water as the wetting solvent. Measurements are reported as average advancing/receding degree ± standard deviation of 12 data points (six measurements each per two samples).

Angle-dependent ESCA data were obtained using a Physical Electronics (PHI) model 5100 spectrometer equipped with a Mg/Ti dual-anode source and an Al/Be window. The system uses a hemispherical analyzer with a single-channel detector. Mg Kα X-rays (1253.6 eV) were used as an achromatic source, operated at 300 W (15 kV and 20 mA). The base pressure of the system was lower than 5×10^{-9} Torr, with an operating pressure no higher than 1×10^{-7} Torr. A pass energy of 89.45 eV was used when obtaining the survey spectra, and a pass energy of 35.75 eV was used for the high-resolution spectra of elemental regions. Spectra were obtained at the following takeoff angles: 15°, 45°, and 90°. The instrument was calibrated using Mg Kα X-radiation: the distance between Au $4f_{7/2}$ and Cu $2p_{3/2}$ was set at 848.67 eV, and the work function was set using Au $4f_{7/2}$ and Cu $2p_{3/2}$ and checked using Au $3d_{5/2}$. All metals were sputter cleaned to remove oxides. Full width at half-maximum for Ag $3d_{3/2}$ was measured to be 0.8 eV at a count rate of 30 000 counts.

External reflectance IR spectra were acquired using a BioRad FTS-40 Fourier transform infrared (FT-IR) spectrometer (BioRad-Digilab, Cambridge, MA) equipped with a Harrick (Ossining, NY) external reflection accessory and a wide band HgCdTe detector. External reflectance spectra of OTS and acrylate-PC thin films on Si were collected at an incidence angle of 60° with respect to the surface normal using 512 scans, triangular apodization, and 4 cm^{-1} resolution. All spectra were acquired with the IR radiation polarized either perpendicular or parallel to the surface normal using a Molectron (Portland, OR) ZnSe wire grid polarizer. Both the perpendicular (R_s) and parallel (R_p) reflection−absorbance spectra were acquired using the respective polarized spectrum of a clean Si wafer as a background. Spectral manipulations performed on the data such as baseline correction and CO_2 peak removal were performed using the Grams/32 software package (Galactic Industries, Salem, NH). Spectral band positions were determined by using a user-written Grams Array Basic program based on a center-of-gravity algorithm.[8]

Molecular orientation calculations were derived from R_p polarized IR spectra using a method developed from classical Fresnel reflection equations[9−12] that was adapted and programmed into Mathcad (Mathsoft, Inc.). The optical constants utilized in the three-phase calculation of molecular orientation were the following: (i) air, $n = 1.0$ and $k = 0.0$; (ii) silicon, $n = 3.4327$ and $k = 0.0$ at 2918 cm^{-1} and $n = 3.4321$ and $k = 0.0$ at 2850 cm^{-1};[13] (iii) OTS, $n_o = 1.48$, $n_e = 1.56$, $k_{bulk} = 0.3$ at 2918 cm^{-1} and $n_o = 1.48$, $n_e = 1.56$, $k_{bulk} = 0.2$ at 2850 cm^{-1}; and (iv) acrylate-PC, $n_o = 1.491$, $n_e = 1.509$, $k_{bulk} = 0.4$ at 2918 cm^{-1} and $n_o = 1.491$, $n_e = 1.509$, $k_{bulk} = 0.3$ at 2850 cm^{-1}.[11,12,14] On the basis of previous studies, a film thickness (h_2) of 18.0 Å was used for the OTS monolayer and a film thickness of 65.5 Å was used for the polymerized PC monolayer.

Vesicle Fusion. Large unilamellar vesicles (LUV) of 10 mM acrylate-PC in 20 mM sodium phosphate buffer (pH 7.4) were prepared by three successive freeze/thaw/vortex cycles using liquid N_2 and a 40 °C water bath. The LUVs were extruded 21 times, each through two back-to-back 2000 nm and then 600 nm polycarbonate filters. The solution was diluted to 1.2 mM with 20 mM sodium phosphate buffer, pH 7.4, and a final salt concentration of 150 mM NaCl was achieved using 750 mM NaCl in water. To a scintillation vial containing either

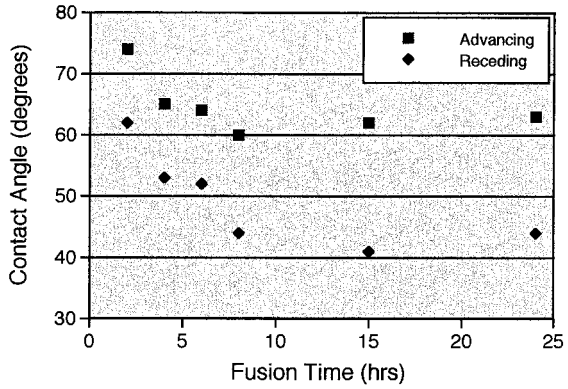

Figure 2. A kinetic study of vesicle fusion to OTS/glass substrates was performed using a 1.2 mM suspension of monoacrylated-PC liposomes in 150 mM NaCl at 37 °C. Advancing and receding contact angles were measured as a function of vesicle fusion time to the alkylated surface followed by a 30 min irradiation interval.

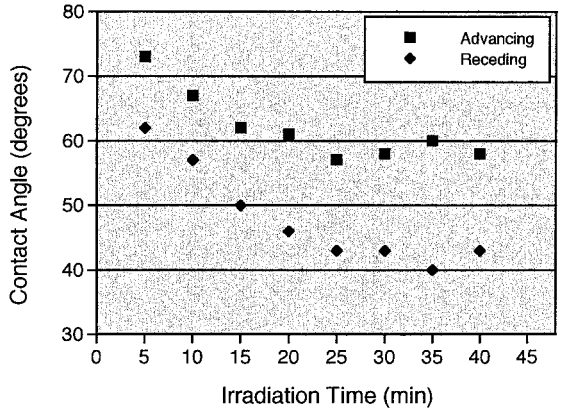

Figure 3. Effect of irradiation time on in-situ polymerization of the supported lipid monolayer. Advancing and receding contact angles were measured as a function of irradiation time under a quartz halogen lamp, which was preceded by a vesicle fusion interval of 15 h.

an OTS-coated glass coverslip or Si wafer, cut to approximately 5 × 10 mm, was added 1 mL of the vesicle solution. The vial was capped and maintained at 37 °C for a specified period of time.

Photopolymerization. A stock solution of co-initiators was prepared as 10 mM EY, 225 mM TEA, and 37 mM VP in water. A 10:1 (mol/mol) monomer:EY ratio (10 μL) was added to the vial containing the vesicle fused substrate from the stock solution via a micropipet and stirred by gentle agitation. The vial was fitted with a septum and purged with N_2 for 15 min. The septum was replaced with Duraseal film and the test sample irradiated from above at a distance of ≈6.5 cm. The light intensity at the substrate surface was measured to be 50 mW/cm^2. Following the photopolymerization period, samples were immediately removed from the polymerization media and washed with water in preparation for subsequent analysis.

Stability Studies. Time-dependent investigations were performed in water at 23 °C in the presence or absence of the surfactant, *n*-octyl-β-glucopyranoside (OG; 1 mM). Samples were incubated for a specified period of time, after which they were removed from the vial, washed with water, dried under a stream of air, and analyzed.

Results and Discussion

A supported phospholipid (acrylate-PC) film was prepared on OTS-coated substrates by vesicle fusion and stabilized by in-situ photopolymerization with visible light. The optimal conditions for film formation were determined with respect to fusion time, irradiation time, and dark time by contact angle analysis. The dependence of surface coverage as a function of vesicle fusion time is presented in Figure 2. In this experiment, irradiation time was held constant at 30 min. A decrease in contact angle was noted over the first 8 h of fusion time followed by a plateau in contact angle values at subsequent time points with average advancing/receding contact angles of 61/43°. These values are similar to those obtained for the free-radical polymerization of acrylate(PC) on OTS glass using AAPD at 70 °C (64/44°). Although polymerization reactions were largely performed in a N_2 atmosphere, similar results were observed when performed in air.

The effect of irradiation time on surface coverage with poly(PC), as determined by contact angle measurements, is presented in Figure 3. Contact angles decreased with increasing duration of irradiation. After a 25 min exposure period, advancing/receding contact angles of 58/42° were observed, with little change noted thereafter. Although shorter irradiation times have been

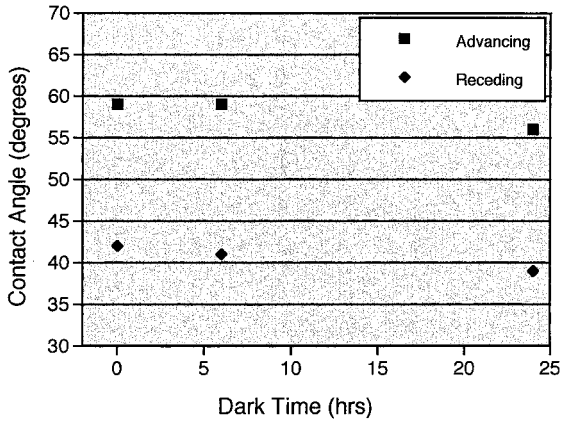

Figure 4. Effect of dark time on in-situ polymerization of the supported lipid monolayer. Advancing and receding contact angles were measured as a function of dark time, which was preceded by 30 min of irradiation interval and a vesicle fusion interval of 15 h.

reported for optimal photopolymerization of other acrylate-containing polymers using EY, this is probably attributable to higher energy fluxes typically associated with the use of argon ion lasers utilized in those reports.[7] The requirement for a longer irradiation period in our system was largely offset by the use of an inexpensive quartz halogen lamp.

"Dark time" is defined as the time necessary to achieve maximum propagation of polymer chains after irradiation has been completed. By leaving the polymerization media static under ambient laboratory conditions, it was determined that the extent of polymerization is unaffected by additional propagation time (Figure 4), at least as can be detected by contact angle analysis. Contact angles remain constant at an average of 58/41° over 0, 6, and 24 h of dark polymerization time. In summary, optimization studies suggested that a 15 h vesicle fusion time, followed by 30 min of irradiation without additional dark time, would yield a fully formed poly(PC) film.

Further definition of atomic level surface properties was provided by angle-dependent ESCA and polarized external reflectance IR spectroscopy. ESCA results are reported in Table 1. Both P and N were identified, providing additional confirmation of a polymerized lipid film. Overall, our results are consistent with values previously reported for PC derivatized glass[2] and a

Table 1. Angle-Dependent ESCA Results for Photopolymerized Phospholipid Monolayer and OTS Glass

	takeoff angle, deg			
	15	45	90	theoret, %
polymer				
C	75.6	64	54.1	79.3
P	0.4	0.9	1.0	0.9
O	20.7	26.8	32.7	16.5
N	1.2	0.9	1.1	0.9
Si	2.0	7.3	11.1	2.4
OTS				
C	74.1	47.7	32.6	81.8
Si	6.9	14.4	19.2	4.6
O	16.1	36.5	47.1	13.6

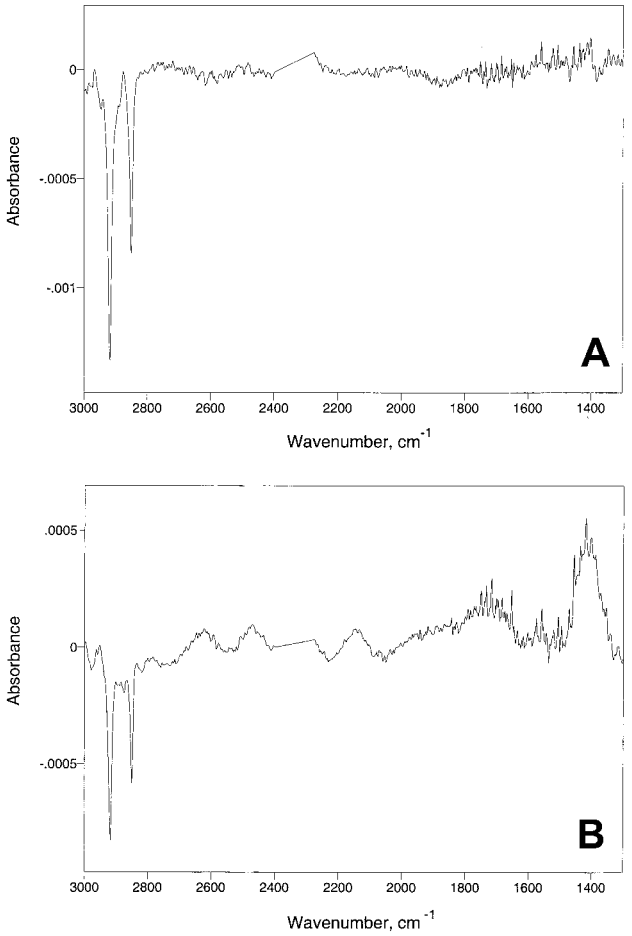

Figure 5. Infrared external reflection−absorption spectra of OTS monolayer film on a silicon substrate. Reflection spectra were acquired with (A) parallel (R_p) and (B) perpendicular (R_s) polarized incoming radiation.

similar thermally polymerized supported lipid film.[4] Although ESCA data afford an unambiguous assessment of the type and atomic percent concentration of surface species, polarized external-reflection IR spectra provide complementary structural information by facilitating an analysis of molecular orientation within these self-assembled ultrathin films. The R_p and R_s polarized reflection IR spectra for an OTS monolayer/Si and a polymerized acrylate-PC film bound to OTS/Si are presented in Figures 5 and 6, respectively. Absorption mode assignments and wavenumber positions calculated from the polarized IR spectra can be found in Table 2.

The R_p and R_s polarized spectra obtained for the OTS monolayer have similar spectral characteristics with

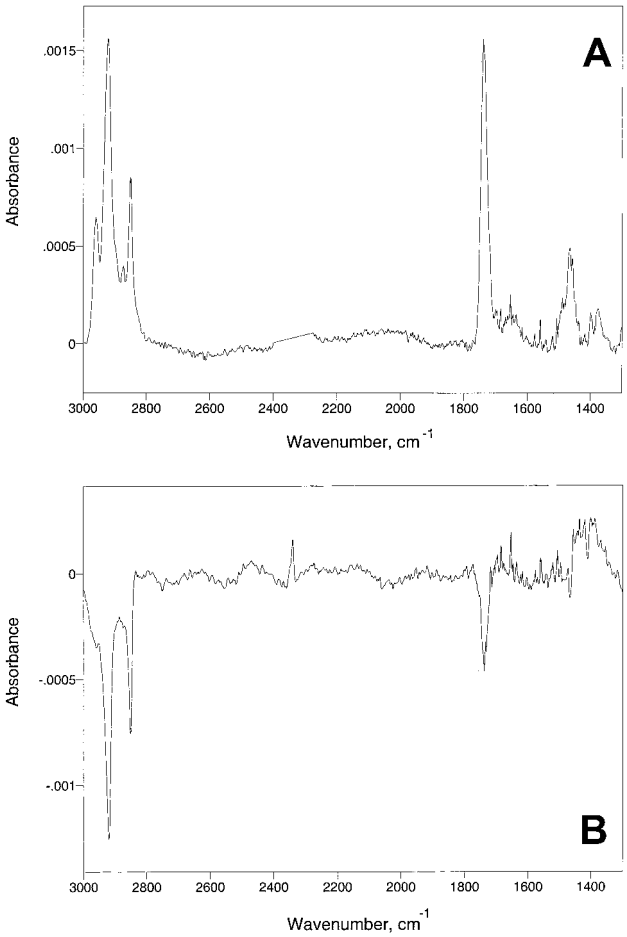

Figure 6. Infrared external reflection−absorption spectra of acrylate-PC film polymerized to OTS monolayer on a silicon substrate. Reflection spectra were acquired with (A) parallel (R_p) and (B) perpendicular (R_s) polarized incoming radiation.

Table 2. External Reflection Infrared Band Assignments

	photopolymerized phospholipid film freq (cm^{-1})		OTS monolayer freq (cm^{-1})	
absorption mode	R_p polarized	R_s polarized	R_p polarized	R_s polarized
$-CH_3$ antisym str	2960.9	2958.7	2946.1	
$-CH_3$ sym str	2872.2			2874.2
$-CH_2$ antisym str	2921.4	2919.0	2917.3	2917.6
$-CH_2$ sym str	2850.5	2851.3	2850.6	2849.8
C=O str	1739.0	1738.9		
CH_2 scissoring	1466.9			
C−O str	1398.5			
$-CH_3$ sym bend	1374.1			

negative absorption bands in the 3000−2800 cm^{-1} region due to the CH stretching modes of the hydrocarbon chains. Negative absorption bands in polarized external reflection IR spectra have been theoretically predicted and experimentally observed in previous investigations of monomolecular films adsorbed onto Si and other semiconductor substrates.[15−19] Although no other notable spectral features are observed, the wavenumber position of the methylene symmetric (ν_s CH_2) and antisymmetric (ν_a CH_2) stretching vibrations can be used as an indicator of hydrocarbon chain order.[20−22] Significantly, average positions of 2917.5 and 2850.2 cm^{-1} for the ν_a CH_2 and ν_s CH_2 stretching bands are indicative of a well-ordered, all-trans conformation of

the hydrocarbon chains in the OTS monolayer.[21,23,24]

The R_p and R_s polarized spectra for the photopolymerized acrylate-PC film bound to OTS/Si are presented in Figure 6. Unlike the OTS polarized spectra, there are distinct differences between the R_p and R_s polarized IR spectra of the acrylate-PC film. All band intensities in the R_p spectrum are positive whereas the band intensities in the R_s spectrum are negative. Moreover, several additional absorption bands are observed in the R_p spectrum. Although both spectra reveal symmetric and antisymmetric CH_3 and CH_2 stretching modes at 3000−2800 cm^{-1} and a C═O stretching mode at 1739.0 cm^{-1}, the CH_2 scissoring vibration at 1466.9 cm^{-1}, the C−O stretching mode at 1398.5 cm^{-1}, and the CH_3 antisymmetric bending mode at 1374.1 cm^{-1} are only observable in the R_p polarized spectrum. Of note, absorption bands due to the PO_2 headgroup (∼1260−1035 cm^{-1}) should be observable in the IR spectrum of the acrylate-PC film. Unfortunately, background interference of the silicon substrate below 1300 cm^{-1} does not allow these vibrations to be resolved.

The presence of both positive and negative band intensities in the external reflection IR spectra of monomolecular films on Si can be explained by consideration of the underlying stratified layer optical physics. In turn, a necessary framework is established for further analysis of macromolecular orientation. Figure 7 illustrates the theoretically expected IR polarized reflection−absorbances for a monomolecular film on a Si substrate at 3000 cm^{-1}. These calculations incorporate the Fresnel reflectance coefficients for the stratified three-layer system and have been described in detail elsewhere. Details of the parameters used in these simulations are given in the caption of Figure 7.[9,15,16,18,19]

In Figure 7A, calculations were performed for the case of both parallel and perpendicular polarized incoming radiation at the air−Si interface. The results show that for perpendicular polarized radiation (i.e., radiation that has its electric vector in the plane of the surface or the *y*-geometric direction in a laboratory-based framework) negative vibrational bands are expected regardless of the incoming angle of incidence of the radiation. In comparison, the direction of the absorbance bands expected for parallel polarized radiation (i.e., radiation that has components of its electric vector both normal to the surface and within the plane of the surface) depends on whether the angle of incidence is below or above the Si Brewster angle at ≈73°. Below this angle, the theoretical p-polarized reflection−absorbance for a monolayer at the Si surface is positive; above 73°, the theoretical p-polarized reflection−absorbance is predicted to be negative.

If these calculations are correct, and negative R_p spectra only occur when the angle of incidence is greater than 73°, how can we account for the negative absorbance bands seen in the R_p spectrum of the OTS monolayer obtained at an incoming angle of 60°? In fact, as mentioned above, when paralled polarized IR radiation is specularly reflected from an interface at nonnormal angles of incidence, the electric field at the surface is a superposition of an electric field component in the plane of the surface (the *x* geometric direction in a laboratory-based framework) in combination with an electric field component normal to the plane of the surface (the *z* geometric direction in a laboratory-based framework). Figure 7B decomposes the theoretical absorbance of the parallel polarized incoming radiation at

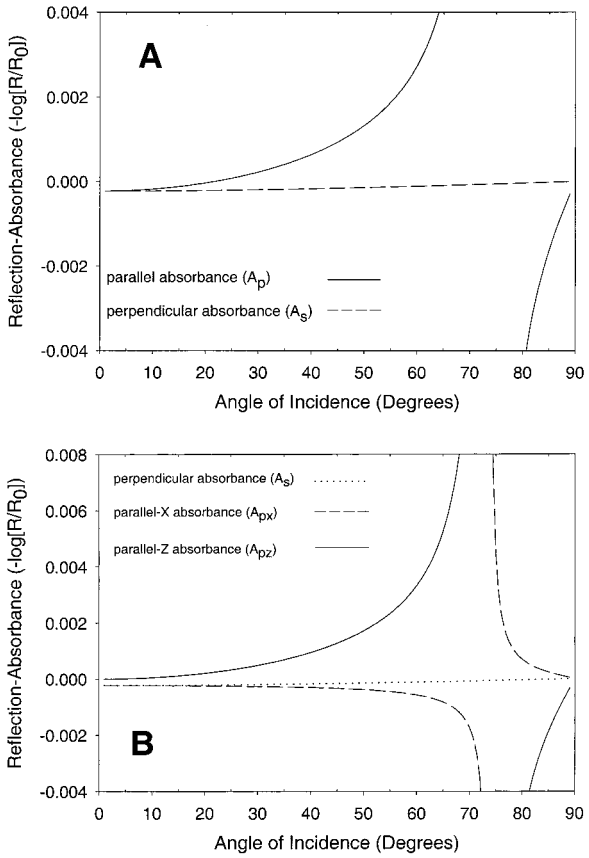

Figure 7. (A) Theoretical reflection−absorbance plot for a monomolecular film at a Si surface. Data were obtained using classical three-phase Fresnel reflectance optical equations with an assumed 25 Å monolayer film at 3000 cm^{-1}. Optical constant data used for monolayer simulations: $n = 1.5$, $k = 0.1$. Optical constants for Si at 3000 cm^{-1} obtained from ref 6. Data were simulated for both parallel and perpendicular polarization of the incoming radiation. Solid line indicates theoretical reflection−absorbance for parallel (A_p) polarized incoming radiation while the dashed line indicates theoretical reflection−absorbance for perpendicular (A_s) polarized incoming radiation. (B) Theoretical reflection−absorbance of the parallel radiation has been decomposed into the components due to the *x*-geometric direction (in the plane of the surface) as well as the *z*-geometric direction (normal to the surface). Solid line represents theoretical reflection−absorbance of parallel polarization, *z* direction (A_{pz}), dashed line represents parallel polarization, *x* direction (A_{px}), and dotted line represents perpendicular (A_s) polarization.

the Si surface into its two component parts using previously published algorithms.[10,25] It is apparent that below the Si Brewster angle all in-plane surface vibrations give rise to negative reflection−absorbance bands (i.e., the theoretical absorbance for perpendicular radiation, A_s, as well as the parallel absorbance in the *x*-direction, A_{px}). Conversely, below 73° vibrational dipole moments that are normal to the surface give rise to positive reflection−absorbances.

A consideration of the individual in-plane and out-of-plane geometric components of the electric fields at the Si surface facilitates additional insights into the detailed structure of anisotropic films on Si. For example, the negative reflection−absorption bands present in the R_p polarized spectrum of the OTS monolayer (Figure 5A) lead us to conclude that the dipole moments of the C−H hydrocarbon vibrations are interacting strongly with the *x*-component of the parallel polarized radiation (Figure 7B). Assuming that the C−H dipole

moment is oriented orthogonal to the chain axis in an all-trans hydrocarbon chain, these IR results, qualitatively speaking, give an orientation of the OTS hydrocarbon chains that is close to the surface normal. This result agrees with the angle-dependent ESCA measurements for the OTS glass monolayer presented in Table 1.

In a similar vein, the polarized IR spectra collected for the acrylate-PC film provide insight into the structural changes that occur after lipid vesicle fusion and polymerization onto the OTS monolayer film. Unlike the R_p polarized spectra for the OTS monolayer, the intensities for the CH_2 and CH_3 vibrations of the R_p polarized spectrum are positive. This indicates that the C−H dipole moments of the hydrocarbon chains in the acrylate-PC film are interacting primarily with the *z*-component of the parallel polarized IR beam (Figure 7B). Any interaction of the hydrocarbon chain C−H dipole moments with electric field components normal to the surface implies an increase in chain tilt angle, probably due to a more disorganized overall monolayer structure.

The average wavenumber positions of the ν_a CH_2 and ν_s CH_2 stretching bands in the acrylate-PC film were measured at 2920.2 and 2850.9 cm^{-1}, respectively (Table 2). This increase in the wavenumber positions for the ν_a CH_2 stretching mode is related to a disordering in the hydrocarbon chains in the acrylate-PC monolayer relative to that of OTS.[21,23,24] This increase in film disorder is also apparent from the change in the average bandwidths of the CH_2 stretching modes (measured at half-height) for the OTS monolayer alone (ν_a $CH_2 = 14.3$ cm^{-1} and ν_s $CH_2 = 11.1$ cm^{-1}), compared to the OTS monolayer on top of which lies a polymerized acrylate-PC film (ν_a $CH_2 = 25.6$ cm^{-1} and ν_s $CH_2 = 15.3$ cm^{-1}).

To quantitatively measure the changes in molecular orientation in the hydrocarbon chains of the OTS and acrylate-PC monolayer films, orientation calculations were performed using the external reflection IR vibrational intensities of the C−H bands in these samples. The methodology used in these calculations has been previously described.[9−12] Briefly, the calculation of molecular orientation in a surface-adsorbed hydrocarbon chain is performed by theoretically simulating a plot of IR reflection−absorbance as a function of dipole moment angle for both the R_p polarized CH_2 symmetric and antisymmetric stretching modes.[11,12] To create the plots of reflection−absorbance vs dipole moment angle, the refractive index (n) and extinction coefficient (k) of the ambient and substrate phases as well as the complex refractive indices (n_o and n_e), k_{bulk}, and thickness of the absorbing thin film must be known. The reflection−absorbance values of the R_p polarized ν_a and ν_s CH_2 stretching modes for the thin film of interest are then used to extrapolate the orientation angle of the dipole moment for each mode. The dipole moment angle of the antisymmetric ν_a CH_2 stretch (α), the dipole moment angle of the symmetric ν_s CH_2 stretch (β), and the molecular orientation angle of the hydrocarbon chain relative to the surface normal (γ) are all orthogonal to one another and are related by the expression

$$\cos^2\alpha + \cos^2\beta + \cos^2\gamma = 1 \qquad (1)$$

Using eq 1 and the optical constants for a three-phase system described in the Experimental Section, the molecular orientations for the OTS and acrylate-PC films were determined to be 21.5° and 46.5°, respectively, relative to the surface normal. The change in molecular orientation from 21.5° to 46.5° shows that the acrylate-PC monolayer, fused and polymerized to the OTS molecules, is more disordered than the OTS monolayer by itself. This conclusion is supported by the increase in the disorder of the hydrocarbon chains in the polymerized acrylate-PC films, as determined by the increase in wavenumber position and bandwidth for the CH_2 stretching modes. The increase of the disorder of the acrylate-PC film is also supported by the negative to positive change in the band intensities of the R_p polarized spectra from 3000 to 2800 cm^{-1} (Figures 5A and 6A), as described above. Further studies directed at determining whether this increased disorder is attributable to multilayer formation, the presence of partially fused vesicles, or related to disorder induced by the polymerization process per se, are ongoing and will be reported in due course.

Table 3. Advancing and Receding Contact Angles (deg) for Substrate Supported Polymerized Phospholipid Films after Incubation in Water

initiator system	initial	1 day	1 week
EY/TEA	57 ± 2/39 ± 1	62 ± 1/40 ± 3	60 ± 1/39 ± 1
AAPD	65 ± 3/46 ± 4	77 ± 4/57 ± 5	79 ± 3/55 ± 2

The relative stability of poly(PC) films produced by either thermal or photopolymerization strategies was characterized in two series of experiments. In the first phase, changes in contact angle were determined following sample incubation in deionized water at 23 °C (Table 3). The photopolymerized film demonstrated little change in contact angle over a 1 week incubation period in water. In contrast, the thermally initiated system exhibited an increase in advancing contact angle of over 10°, which may be attributable to the generation of a higher proportion of oligomers and/or low molecular weight polymer chains when a self-assembled lipid film is polymerized under these conditions. Paradoxically, others have reported relatively high number-average polymer molecular weights when lipid vesicles are polymerized at temperatures above the T_m of the lipid monomer.[26,27] This observation has been related to both enhanced lateral diffusion of the lipid species and improved permeability of the free-radical initiator into the lipid bilayer. Thus, our observations suggest that the assembly of lipids onto a solid support likely has a significant impact upon the effectiveness of a given polymerization scheme. Recently, we have documented that the stability of a supported lipid monolayer is compromised at temperatures exceeding the lipid T_m with significant loss of substrate supported lipid molecules.[5] Consequently, monomer loss probably occurs throughout a thermally initiated polymerization process which proceeds over a relatively long reaction period at a temperature exceeding the melting point of the acrylated lipid. Since the number-average degree of polymerization of monoacrylated lipids in bilayers has been reported proportional to $[M]^2$, surface loss of lipid may have a profound impact on polymer molecular weight.[26a] Although a change in the phase state of the lipid monolayer does not establish a mechanism for lipid loss, several investigators have documented spontaneous thermodynamic rearrangement of phosphatidylcholine molecules in favor of structures with smaller radii of curvature upon input of thermal,[28] chemical,[29] or mechanical energy.[30] Therefore, with an increase in temperature, vesicles may be generated and subsequently lost from the lipid monolayer. We believe that

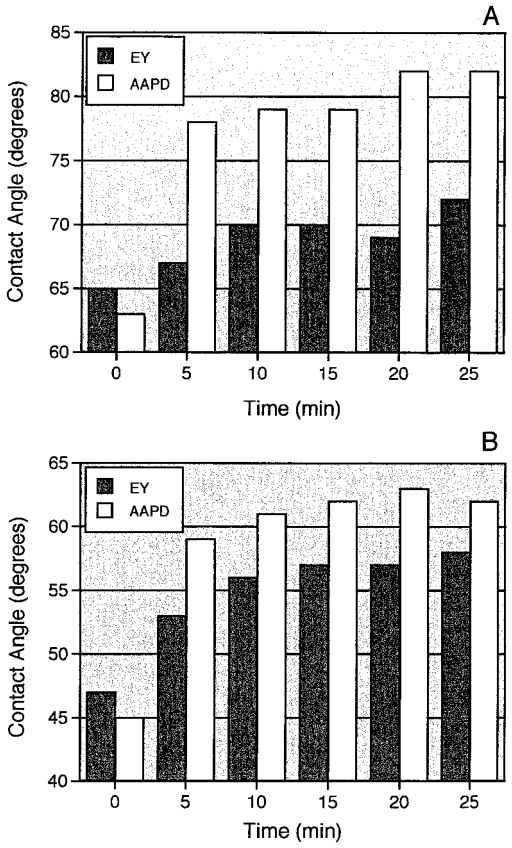

Figure 8. Effect of *n*-octyl-*β*-glucopyranoside (1 mM) on the stability of the supported lipid monolayer. Advancing (A) and receding (B) contact angles were measured as a function of incubation time.

visible-light-mediated polymerization at a temperature below that required for a thermally initiated reaction has permitted us to circumvent the problem of local monomer loss from the supporting substrate.

Polymer desorption occurs when a displacing moiety, such as a solvent, solvent mixture, surfactant, or other polymer, replaces established polymer−surface contacts. Since high molecular weight polymer chains have a greater adsorption energy than their lower molecular weight analogues by virtue of increased surface contacts, it follows that the lower molecular weight polymers are more easily desorbed, all other factors being equal. In the final phase of stability analysis, OG was used as a displacer molecule for the desorption of supported lipid films. A rapid increase in contact angle, followed by a plateau region at longer incubation times, was observed for both thermal and photopolymerized samples (Figure 8). Nonetheless, both the rate of rise in contact angle and the final plateau values obtained for the heat-initiated system are indicative of accelerated desorption, probably as a consequence of shorter polymer chains.

Summary

A stabilized, phosphatidylcholine-containing polymeric surface was produced by in-situ photopolymerization of 1-palmitoyl-2-[12-(acryloyloxy)dodecanoyl]-*sn*-gycero-3-phosphorylcholine at a solid−liquid interface. The phospholipid monomer was synthesized, prepared as unilamellar vesicles, and fused onto a close-packed monolayer of octadecyltricholorosilane on glass. Free-radical polymerization was carried out in aqueous solution under physiologically benign conditions using the eosin Y/triethanolamine initiating system. The supported monolayer displayed advancing and receding water contact angles of 58° and 41°, respectively. ESCA data were consistent with the formation of a supported lipid film. External reflectance IR spectroscopy, however, demonstrated a change in hydrocarbon chain orientation from 21.5° to 46.5° for an OTS monolayer supporting a fused and polymerized acrylate-PC film, which reflects an increase in molecular disorder. In the absence of network formation, photopolymerized films demonstrated stability that was superior to that observed for polymeric monolayers produced by a thermally initiated free-radical process.

Acknowledgment. This work was supported by grants from the NIH (GM40117 R.A.D. and HL56819 E.L.C.), the Juvenile Diabetes Foundation International, and the Molecular Design Institute at the Georgia Institute of Technology. The authors acknowledge the Emory University Mass Spectrometry Center provided by grants from the NIH and NSF, Professor Joseph A. Gardella, Jr., and Dr. Richard Nowak at SUNY Buffalo for ESCA measurements and helpful discussions with Professor Loren Tolbert at the Georgia Institute of Technology.

References and Notes

(1) (a) Hayward, J. A.; Chapman, D. *Biomaterials* **1984**, *5*, 135−142. (b) Hall, B.; Bird, R. R.; Kojima, M.; Chapman, D. *Biomaterials* **1989**, *10*, 219−24. (b) Ishihara, K.; Tsuji, T.; Kurosaki, T.; Nakabayashi, N. *J. Biomed. Mater. Res.* **1994**, *28*, 225−32.

(2) (a) Hayward, J. A.; Durrani, A. A.; Lu, Y.; Clayton, C. R.; Chapman, D. *Biomaterials* **1986**, *7*, 252. (b) Kohler, A. S.; Parks, P. J.; Moorradian, D. L.; Rao, G. H. R.; Furcht, L. T. *J. Biomed. Mater. Res.* **1996**, *32*, 237−242. (c)Van der Heiden, A. P.; Goebbels, D.; Pijpers A. P.; Koole, L. H. *J. Biomed. Mater. Res.* **1997**, *37*, 282. (d) Yang, Z.; Yu, H. *Langmuir* **1999**, *15*, 1731.

(3) (a) Ueda, T.; Oshida, H.; Kurita, K.; Ishihara, K.; Nakabayashi, N. *Polymer J.* **1992**, *24*, 1159−1269. (b) Ishihara, K.; Hanyuda, H.; Nakabayashi, N. *Biomaterials* **1995**, *16*, 873. (c) Ishihara, K.; Ziatz, N. P.; Tierney, B. P.; Nakabayashi, N. *J. Biomed. Mater. Res.* **1997**, *25*, 1397−1407. (d) Ruiz, L.; Hilborn, J. G.; Leonard, D.; Mathieu, H. J. *Biomaterials* **1998**, *19*, 987−998. (e) Campbell, E. J.; O'Byrne, V.; Stratford, P. W.; Quirk, I.; Vick, T. A.; Wiles, M. C.; Yianni, Y. P. *ASAIO J.* **1994**, *40*, M853. (f) Yamada, M.; Li, Y.; Nakaya, T. *J. Macromol. Sci., Pure Appl. Chem.* **1995**, *A32*, 1723−1733. (g) Li, Y.-J.; Matthews, K. H.; Chen, T.-M.; Wang, Y.-F.; Kodama, M.; Nakaya, T. *Chem. Mater.* **1996**, *8*, 1441−1450. (h) Chen, T. M.; Wang, Y. F.; Li, Y. J.; Nakaya, T.; Sakurai, I. *J. Appl. Polym. Sci.* **1996**, *60*, 455−464.

(4) (a) Marra, K. G.; Winger, T. M.; Hanson, S. R.; Chaikof, E. L. *Macromolecules* **1997**, *30*, 6483−6488. (b) Marra, K. G.; Kidani, D. D. A.; Chaikof, E. L. *Langmuir* **1997**, *13*, 5697−5701. (c) Chon, J. H.; Marra, K. G.; Chaikof, E. L. *J. Biomater. Sci. Polym. Ed.* **1999**, *10*, 95−108.

(5) Winger, T. M.; Ludovice, P. J.; Chaikof, E. L. *Langmuir* **1999**, *15*, 3866−3874.

(6) Valdes-Aguilers, O.; Pathak, C. P.; Shi, J.; Watson, D.; Neckers, D. C. *Macromolecules* **1992**, *25*, 541−547.

(7) (a) Pathak, C. P.; Sawhney, A. S.; Hubbell, J. A. *J. Am. Chem. Soc.* **1992**, *114*, 8311−8312. (b) Cruise, G. M.; Hegre, O. D.; Scharp, D. S.; Hubbell, J. A. *Biotechnol. Bioeng.* **1998**, *57*, 65S−665.

(8) Cameron, D. G.; Kauppinen, J. K.; Moffatt, D. J.; Mantsch, H. H. *Appl. Spectrosc.* **1982**, *36*, 245−250.

(9) Hansen, W. N. *J. Opt. Soc. Am.* **1968**, *58*, 380−390.

(10) Hansen, W. N. *Symp. Faraday Soc.* **1970**, *4*, 27−35.

(11) Hasegawa, T.; Takeda, S.; Kawaguchi, A.; Umemura, J. *Langmuir* **1995**, *11*, 1236−1243.

(12) Sakai, H.; Umemura, J. *Bull. Chem. Soc. Jpn.* **1997**, *70*, 1027−1032.

(13) Edwards, D. F. Silicon. In *Handbook of Optical Constants of Solids*; Palik, E. D., Ed.; Academic Press: Orlando, FL, 1985.

(14) Ducharme, D.; Max, J. J.; Salesse, C.; Leblanc, R. N. *J. Phys. Chem.* **1990**, *94*, 1925−1932.
(15) Allara, D. L.; Baca, A.; Pryde, C. A. *Macromolecules* **1978**, *11*, 2215−2220.
(16) Dluhy, R. A. *J. Phys. Chem.* **1986**, *90*, 1373−1379.
(17) Wong, J. S.; Yen, Y.-S. *Appl. Spectrosc.* **1988**, *42*, 598−604.
(18) Mielczarski, J. A.; Yoon, R. H. *J. Phys. Chem.* **1989**, *93*, 2034−2038.
(19) Yen, Y.-S.; Wong, J. *J. Phys. Chem.* **1989**, *93*, 7208−7216.
(20) Tasumi, M. S.; Miyaza, T. J. *J. Mol. Spectrosc.* **1962**, *9*, 261.
(21) Snyder, R. G.; Hsu, S. L.; Krimm, S. *Spectrochim. Acta, Part A* **1978**, *34A*, 395−406.
(22) Painter, P. C. C.; M. M.; Koenig, J. L. *The Theory of Vibrational Spectroscopy and its Application to Polymeric Materials*; John Wiley & Sins: New York, 1982.
(23) Snyder, R. G.; Strauss, H. L.; Elliger, C. A. *J. Phys. Chem.* **1982**, *86*, 5145−5150.
(24) MacPhail, R. A.; Strauss, H. L.; Snyder, R. G.; Elliger, C. A. *J. Phys. Chem.* **1984**, *88*, 334−341.
(25) Hansen, W. N. Internal reflection spectroscopy in electrochemistry. In *Advances in Electrochemistry and Electrochemical Engineering*; Muller, R. H., Ed.; J. Wiley-Interscience: New York, 1973; Vol. 9, pp 1−60.
(26) (a) Sells, T. D.; O'Brien, D. F. *Macromolecules* **1994**, *27*, 226−233. (b) Clapp, P. J.; Armitage, B. A.; O'Brien, D. F. *Macromolecules* **1997**, *30*, 32−41. (c) Sisson, T. M.; Srisiri, W.; O'Brien, D. F. *J. Am. Chem. Soc.* **1998**, *120*, 2322−2329. (d) Hub, H.-H.; Hupfer, B.; Koch, H.; Ringsdorf, H. *Angew. Chem., Int. Ed. Engl.* **1980**, *19*, 938. (e) Ringsdorf, H.; Schlarb, B.; Venzmer, J. *Angew. Chem., Int. Ed. Engl.* **1988**, *27*, 113−158. (f) Batchelder, D. N.; Evans, S. D.; Freeman, T. L.; Haussling, L.; Ringsdorf, H.; Wolf, H. *J. Am. Chem. Soc.* **1994**, *116*, 1050. (g) Tsibouklis, J.; Feast, J. W. *TRIP* **1993**, *1*, 16. (h) Singh, A.; Markowitz, M. A. In *Novel Techniques in Synthesis of Processing of Advanced Materials*; Singh, J., Copley, S. M., Eds.; 1995; pp 177−186. (i) Einaga, Y.; Sato, O.; Iyoda, T.; Fujishima, A.; Hashimoto, K. *J. Am. Chem. Soc.* **1999**, *121*, 3745−3750.
(27) Lei, J.; Sisson, T. M.; Lamparski, H. G.; O'Brien, D. F. *Macromolecules* **1999**, *32*, 73−78.
(28) (a) New, R. R. C. *Liposomes: A Practical Approach*; Oxford University Press: New York, 1992. (b) Lipowsky, R. *Curr. Opin. Struct. Biol.* **1995**, *5*, 531−540.
(29) Batzri, S.; Korn, E. D. *Biophys. Acta* **1973**, *298*, 1015−1019.
(30) (a) Olson, F.; Hunt, C. A.; Szoka, F. C.; Vail, W. J.; Papahadjopolous, D. *Biochim. Biophys. Acta* **1979**, *557*, 9−23. (b) Mayer, L. D.; Hope, M. J.; Cullis, P. R. *Biochim. Biophys. Acta* **1986**, *858*, 161−168. (c) MacDonald, R. C.; MacDonald, R. I.; Menco, B. P. M.; Takashita, K.; Subbarao, N. K.; Hu, L.-R. *Biochim. Biophys. Acta* **1991**, *1061*, 297−303. (d) Clerc, S. G.; Thompson, T. E. *Biophys. J.* **1994**, *67*, 475−477.

MA9915780